CRYSTALLOGRAPHIC, MORPHOLOGICAL AND W-H MODELS INVESTIGATIONS ON Mn SUBSTITUTED ZnO NANOCRYSTALS

V. Mote and B. Dole*

* drbndole.phy@gmail.com

Advanced Materials Research Laboratory, Department of Physics, Dr. Babasaheb Ambedkar Marathwada University, Aurangabad, India.

Abstract: *Mn doped ZnO nanocrystals were prepared by co-precipitation route sintered at 450 °C temperature. XRD results indicate that the samples having hexagonal (wurtzite) structure. From X-ray data it is found that the lattice parameters increase with increasing Mn concentration. The X-ray density decreases with increasing Mn concentration of $Zn_{1-x}Mn_xO$ nanocrystals. It indicates that the Mn ions go into the Zn site in the ZnO lattice structure. TEM results reveal that the pure and Mn substituted ZnO samples are spherical in shape with average particle size about 20-60 nm. The crystalline size and lattice strain were evaluated by Williamson-Hall (W-H) analysis using X-ray peak broadening*
data. All other relevant physical parameters such as strain, stress and energy density were calculated by the different models Viz, uniform deformation model (UDM), uniform deformation stress model (UDSM) and Uniform deformation energy density model (UDEDM) considering the Williamson-Hall analysis. These models reveal different strain values it may be due to the anisotropic nature of the material. It is found that the mean particle size of $Zn_{1-x}Mn_xO$ nanoparticles was estimated from TEM analysis, Scherrer's formula & W-H analysis is highly comparable.

Keywords: *Nanocrystals; Co-precipitation route; TEM; UDEDM.*

1. INTRODUCTION

Diluted magnetic semiconductor is a very important field for the ongoing research activity among the materials scientists, technocrats and industrialists. The diluted magnetic semiconductor particles exhibit size-dependant properties, namely scaling of the energy band gap and also change for optical properties. Therefore, they are considered as the front runners for technological applications. Zinc oxide is a II–VI semiconductor with large band gap (E_g=3.37 EV). It has higher exciton binding energy (60 meV). Zinc oxide has been used in numerous applications like photo catalysis [1], gas sensors [2], Varistors [3] and low-voltage phosphor materials [4] and so on. Due to its unique properties in structures, ZnO is the richest family of nanostructures among all the semiconductors [5].

Crystals are not prefect owing to their finite size, but the perfect crystal will extend due to deviation from perfect crystalline gets diffraction peaks broadening. Two important properties of crystals are outlined a) crystallite size and b)

lattice strain. Both the properties are described at length. a) Crystallite size is a measure of the size of coherently diffracting domain size. Crystallite size is not the same as diffracting domain size.

Crystallite size is not the same as the particle size owing to the presence of polycrystalline aggregates [6]. Scanning electron microscopy (SEM), TEM analysis Brunauer Emmett Teller (BET), light (laser) scattering experiment is being used for the measurement of the particle size. These techniques are generally used to measure the particle size. b) Lattice strain is a measure of lattice parameter distribution which gets from crystal imperfections. The strain has the same sources such as coherency stresses, sinter stresses, grain boundary, triple junction and stacking faults [7]. The dislocation distribution is studied by the X-ray line broadening. W-H method is used for the estimation of size and strain because it is the integral breadth and owing to this it is used for estimation of strain and other related parameters. A comparative determination of the mean particle size of ZnO nanoparticles obtained by TEM and XRD technique is studied

at length. The strain associated with the annealed Mn substituted ZnO samples at 450 °C owing to lattice deformation were estimated using UDM. The W-H modified models, namely USDM and UDEDM reveal the information about stress and strain. The UDM gives the isotropic nature of the crystal whereas other two models describe the anisotropic nature of the crystal. We report such investigations on pure and Mn substituted ZnO nanoparticles synthesized by the co precipitation method in this paper at length.

2. EXPERIMENTAL

2. 1. Materials

Zinc acetate dihydrate $Zn(CH_3COO)_2.2H_2O$ (99+% A. R. Grade, Kemphasol, India), Manganese acetate tetrahydrate $Mn(CH_3COO)_2.4H_2O$ (99+% A. R. Grade, Kemphasol, India), Potassium hydroxide (KOH) (A. R. Grade, sdFiNE-CHEM Limited, India) and methanol were used as starting materials.

2. 2. Characterization Techniques

X-ray diffraction was used to investigate the structural parameters. TEM was in force to determine the shape and size of the prepared samples in order to understand the enhanced properties of annealed pure and Mn substituted ZnO nanocrystals. Structural parameters of the samples were investigated by powder X-ray diffraction (Model: PW-3710) using CuKα radiation ($\lambda = 1.5406$ Å). To study the sample morphology, the powders were ultrasonically mixed with ethanol and suspended in a Cu mesh, which was the sample holder of a transmission electron microscope (TEM) operated at 200 kV (TEM- Model CM 200, SUPERTWIN). Crystallite size and lattice strain were determined using Scherrer's formula and the Williamson–Hall (W–H) analysis.

2. 3. Sample Preparation

Samples of $Zn_{1-x}Mn_xO$ were prepared by the reaction of Zn^{2+} and OH- in an alcoholic medium (methanol) at low temperature. Zinc acetate

dihydrate $Zn(CH_3COO)_2.2H_2O$, Manganese acetate tetrahydrate $Mn(CH_3COO)_2.4H_2O$, Potassium hydroxide (KOH) and methanol were used as starting materials. In this procedure for pure ZnO, two solutions, one containing Zinc acetate dihydrate $Zn(ac)_2.2H_2O$ was dissolved in 100 ml Methanol and other containing KOH in 100 ml methanol was prepared and aided by magnetic stirring while heating at 325 K for 2h. The KOH solution was added to the solution containing $(Zn(ac)_2.2H_2O)$ with constant stirring while heating at 325K for 2 h, it was aged for two days. The precipitate which formed was separated from the solution by filtration, washed several times with distilled water and absolute ethanol and then dried in air at 400 K to obtain ZnO nanocrystalline powders. The nanocrystalline sample was annealed at 683 K for 8h in the air. Similarly, for the synthesis of Mn substituted ZnO, two solutions, one containing 1M Zinc acetate dihydrate and Manganese acetate tetrahydrate was dissolved in 100 ml of methanol and other containing KOH were dissolved in 100 ml methanol separately and stirred it at 325 K for 2h. The KOH solution was then added to the solution containing $(Zn(ac)_2.2H_2O)$ and Manganese acetate with constant stirring at 325K for 2h and then it was aged for two days. The precipitate formed were separated from the solution by filtration, washed several times with distilled water and absolute ethanol and then dried in air at 400 K to obtain pure ZnO and ZnMnO nanopowders. The nanocrystalline samples obtained were annealed in air for 8 h at 450 °C.

3. RESULTS AND DISCUSSION

3. 1. Structural Parameters

Figure 1 shows XRD patterns for pure and Mn substituted ZnO samples. The XRD data shows that the as prepared $Zn_{1-x}Mn_xO$ nanocrystals having wurtzite structure. No extra diffraction peaks corresponding to Zn, Zn (OH$_2$) or other ZnO phases were detected which indicate that the purity and Mn substituted ZnO nanocrystals are monophasic. The peak intensity of the $Zn_{1-x}Mn_xO$ samples was sharp and narrow which confirms
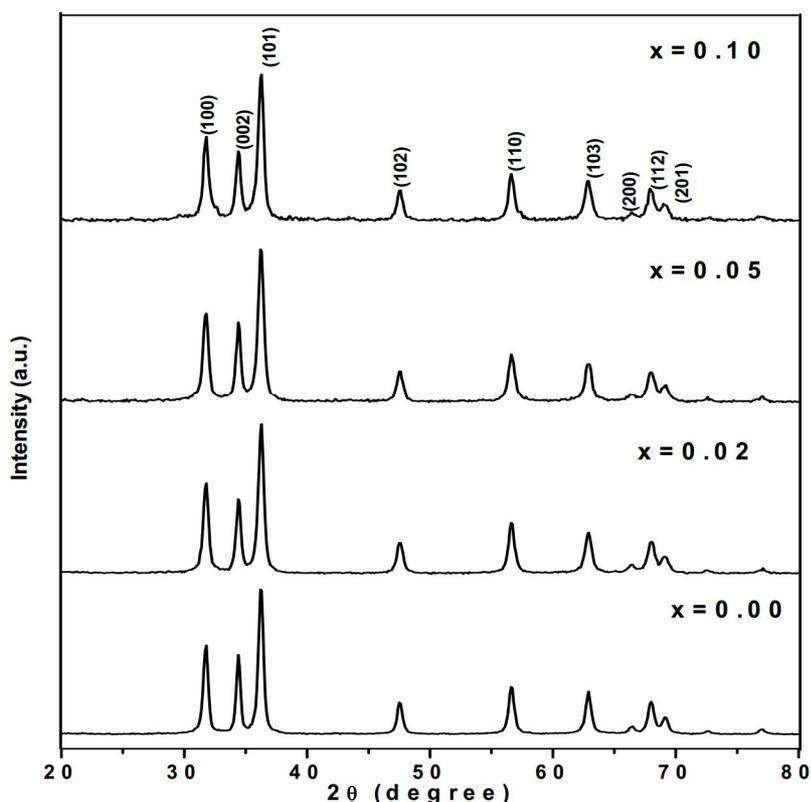
Fig. 1. X-ray diffraction of $Zn_{1-x}Mn_xO$ nanocrystals

that the samples are in high quality with good crystallinity and fine grain size. The lattice parameters were calculated using XRD data. It is found that the lattice parameters increase with increasing Mn concentration. It indicates that the Mn ions go to the Zn site in ZnO structure. The volume of the unit cell was evaluated using the lattice parameters. It was observed that the volume of unit cell increases with increasing Mn content. It may be due to the smaller ionic radii of Zn (0.74 A⁰) ions as compared to Mn (0.80 A⁰) ions. The X- ray density was calculated using XRD data. It is found that X-ray density reduces with increasing Mn concentration; it may be due to the reduction in molecular weight as well as increasing the volume of unit cell. The lattice parameters, volume of the unit cell and X-ray density are listed in table 1.

3. 2. Size and Strain of Crystallites

The peak broadening reflects grain refinement

alongwith large strain is associated with the powder. The instrumental broadening β_{hkl} of each diffraction peak of $Zn_{1-x}Mn_xO$ nanocrystals was corrected using the following relation.

$$\beta_{hkl}=[(\beta_{hkl})^2{}_{Measured}-(\beta_{hkl})^2{}_{Instrumental}]^{1/2} \qquad (1)$$

Table 1. The lattice parameters, volume of unit cell and X-ray density of Mn substituted ZnO nanocrystals synthesized by co-precipitation route.

Samples	a (A⁰)	c (A⁰)	Volume (A⁰)³	X- density (g/cm³)
0.00	3.2491	5.2063	47.5977	5.6802
0.02	3.2497	5.2071	47.6226	5.6626
0.05	3.2509	5.2088	47.6733	5.6347
0.10	3.2512	5.2092	47.6858	5.5969

Table 2. Geometrical parameters of annealed $Zn_{1-x}Mn_xO$ nanocrystals at 450 0C.

Samples (x)	Scherrer's method D (nm)	W-H Method									TEM Particle size (nm)
		UD M		UDSM			UDEDM				
		D (nm)	ε X 10^{-4}	D (nm)	σ (MPa)	ε X 10^{-4}	D (nm)	U (kJm$^-$)	σ (MPa)	ε X 10^{-4}	
0.00	29.81	31.87	0.00095	32.78	129	0.00102	32.47	50	125	0.00098	20-60
0.02	25.57	29.69	0.00134	30.81	182	0.00143	30.40	70	148	0.00116	-
0.05	25.51	27.19	0.00124	28.65	177	0.00139	28.07	67	145	0.00114	-
0.10	20.54	26.92	0.00109	27.40	144	0.00113	27.29	45	119	0.00094	20-50

Using the Debye-Scherrer's formula, the average crystalline size was evaluated

$$D = \frac{K\lambda}{\beta_{hkl} \, Cos\, \theta} \tag{2}$$

Where D is the crystalline size, K is the shape factor (0.9), λ is the wavelength of Cuk$_\alpha$ radiation, β_{hkl} is the instrumental corrected integral breadth of the reflection (in radians) located at 2θ and θ is the angle of reflection (in degree) was employed to relate the crystalline size of the line broadening. From the calculations, the average crystalline size of the pure and Mn substituted ZnO nanoparticles was

investigated in the range 20-30 nm and tabulated in table 2. From table 2, it can be seen that the average crystallite size decreases with increasing Mn content. It may due to the small grain growth of Mn substituted ZnO nanocrystals as comprised to pure ZnO nanocrystals.

Owing to crystal imperfection and distortion, the strain induced in the sample was calculated by the formula [8].

$$\varepsilon = \frac{\beta_{hkl}}{4 \tan \theta} \tag{3}$$

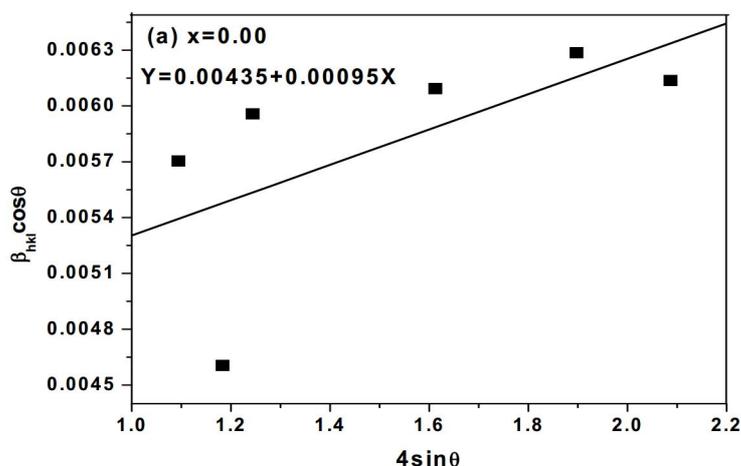It is noticed from equations (2) & (3), the peak width of crystallite size varies as 1/cosθ whereas
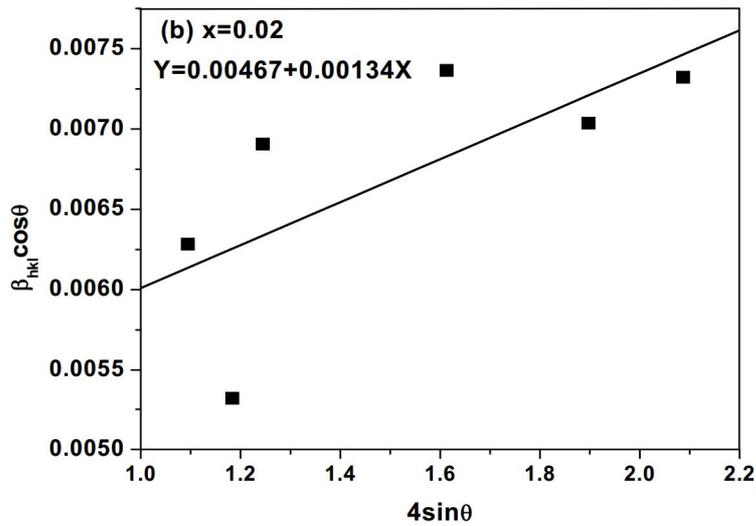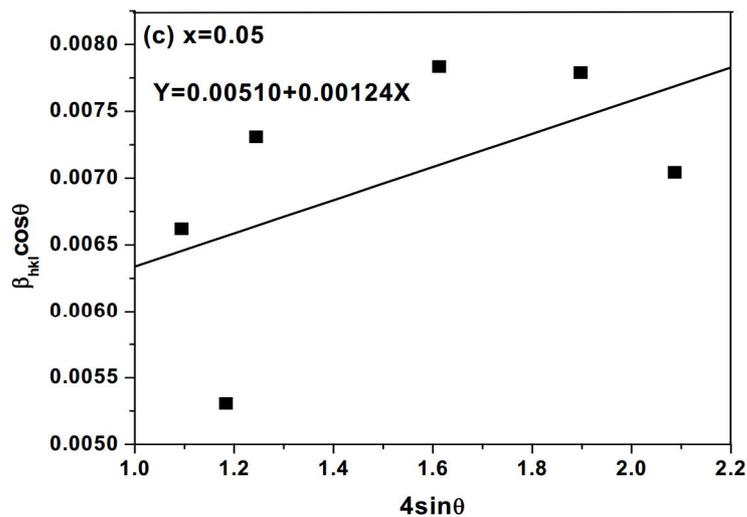

Fig. 2(a).

Fig. 2(b).

Fig. 2(c).

strain varies as tanθ.

Considering the particle size is not related to strain it means that both are independent of each other and they have Cauchy like profile. Williamson-Hall formulated a method of size and strain broadening by observing at the peak width as a function of diffracting angle 2θ and revealed the relation by adding an equation (2) with equation (3). One gets an observed line breadth.

$$\beta_{hkl} = \frac{K\lambda}{D\cos\theta} + 4\varepsilon\tan\theta \qquad (4)$$

For getting $\beta_{hkl}\cos\theta$, multiplying by $\cos\theta$ both sides and simplifying equation in the following form:

79
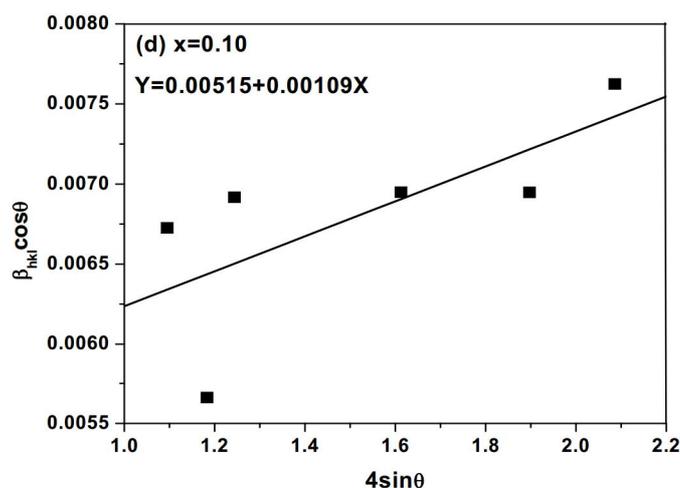
Fig. 2(d).

Fig. 2(a-d). Plots of β_{hkl} cosθ Vs 4Sinθ of $Zn_{1-x}Mn_xO$ samples.

$$\beta_{hkl} \cos\theta = \frac{K\lambda \cos\theta}{D \cos\theta} + 4\varepsilon \frac{\sin\theta}{\cos\theta} x \cos\theta$$

$$\beta_{hkl} \cos\theta = \frac{K\lambda}{D} + 4\varepsilon \sin\theta \qquad (5)$$

Equation (5) is known as a uniform deformation model (UDM). These equations are the W–H equations. Figure 2(a-d) shows the plots of β_{hkl}cosθ versus 4sinθ for pure and Mn substituted ZnO nanocrystals. The lattice corresponding to those peaks are (100), (002), (101), (102), (110) & (103). From the linear fit to the data the crystalline size was estimated from the Y-intercept and the strain ε from the slope of the fit. In UDM the strain was considered to be uniform in all crystallographic directions. The isotropic nature of the crystal is considered, where the material properties are independent of direction along which they are measured. Figure 2(a-d) confirms the UDM for $Zn_{1-x}Mn_xO$ nanocrystals, the lattice strain first increases for x= 0.02 and then decreases with increasing Mn content.

The lattice strain versus Mn concentration is shown in figure 3. The average crystallite size is in the range of 26 - 32 nm. The strain and average crystallite size are tabulated in table 2.

Uniform deformation stress and uniform deformation energy density models were referred to understand the anisotropic nature of young's modulus of the crystals is more realistic [9, 10]. Using Hooke's law, the linear proportionality was maintained between the stress and strain i.e. σ = Eε. It is confirmed that the stress is directly proportional to the strain ε, where E is a proportionality constant or the elasticity or Young's modulus. By putting the value of ε in equation (5), W-H equation is modified.

$$\beta_{hkl} \cos\theta = \frac{K\lambda}{D} + 4 \sin\theta \, \sigma/E_{hkl} \qquad (6)$$

Here E_{hkl} is perpendicular to the set of the crystal lattice plane (hkl). The equation (6) is called as a uniform deformation stress model (UDSM). Figure 4(a-d) shows β_{hkl}cosθ against 4sinθ/E_{hkl} plots for the samples. The uniform stress is determined using slope of the plots and crystalline size D is obtained from the intercept of the plots. If one knows the value of E_{hkl} of hexagonal ZnO structure, then strain ε can be determined. The young's modulus Ehkl [11, 12] is concerned with their elastic compliances S_{ij} for
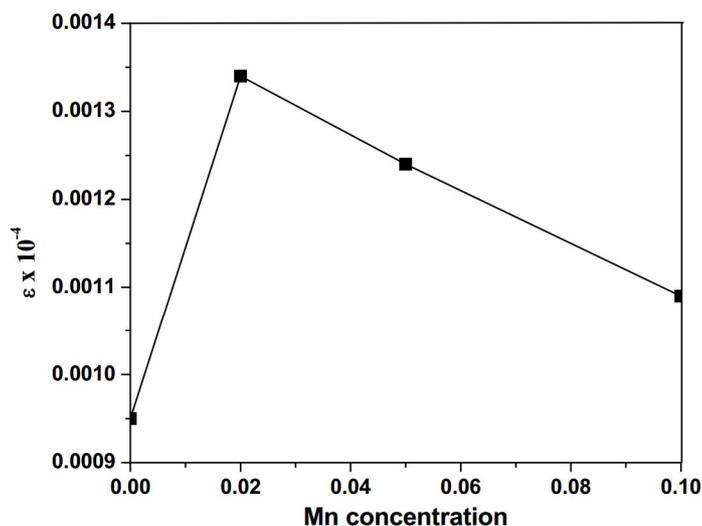
80

Fig. 3. Lattice strain versus Mn concentration of $Zn_{1-x}Mn_xO$ samples.

wurtzite structural sample i.e.

$$\beta_{hkl}\cos\theta = \frac{K\lambda}{D} + \langle 4\sin\theta(2u/E_{hkl})^{1/2}\rangle \qquad (7)$$

Where S_{11}= 7.858 X10^{-12}, S_{13}= -2.206 X 10^{-12}, S_{33}= 6.940X10^{-12}, S_{44}=23.57 X10^{-12} m²N^{-1} are the elastic compliances of ZnO [13]. Figure 3 shows the UDSM for pure and Mn substituted ZnO nanocrystals. The uniform deformation stress is obtained by plotting β_{hkl} cosθ versus 4sinθ/E_{hkl} from the slope of line and using the value of lattice strain. From UDSM model the stress is decreased with increasing Mn content and also the lattice strain decreases with increasing Mn content. It may be due the decreasing average crystallite size.

The average crystallite size is in the range of 27-33 nm. The values of lattice strain, stress and average crystallite size are tabulated in table 2.

Whereas the values of these parameters in reported literature are higher [14].

The homogeneous isotropic nature of the crystal is reflected by the equation (5). But it is not accessible for many cases, the hypothesis of homogeneity and isotropy is not satisfied. It is noticed that the all proportionality constants associated with the stress-strain relation are no longer independent when the strain energy density u. It is well known that the elastic system follows the Hooke's law, the energy density u (energy per unit volume) can be written using following relation u = ε²E_{hkl}/2. The modified form of equation (6) is as under where u is the energy density.

The equation (8) is known as Uniform deformation energy density model (UDEDM). The W–H relation is modified assuming UDEDM and the corresponding plots are shown in figures 6 (a-d). The energy density of

$$E_{hkl} = \frac{[h^2 + (h+2k)^2/3 + (al/c)^2]^2}{S_{11}(h^2 + (h+2k)^2/3 + S_{33}(al/c)^4 + (2S_{13} + S_{44})(h^2 + (h+2k)^2/3(al/c)^2} \qquad (8)$$

Fig. 4(a).

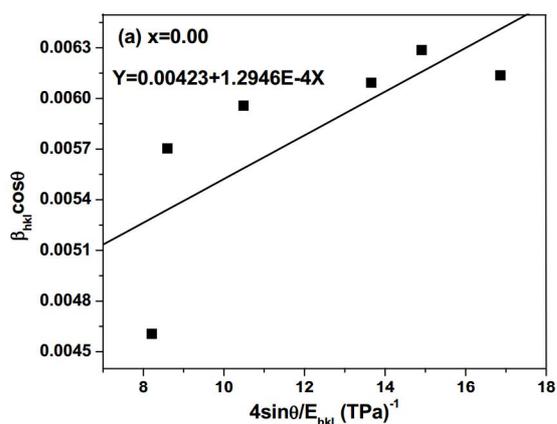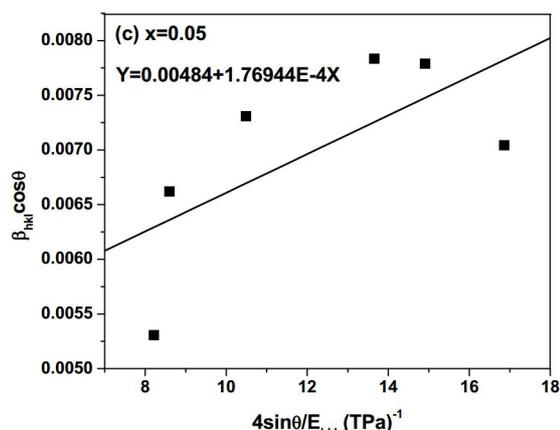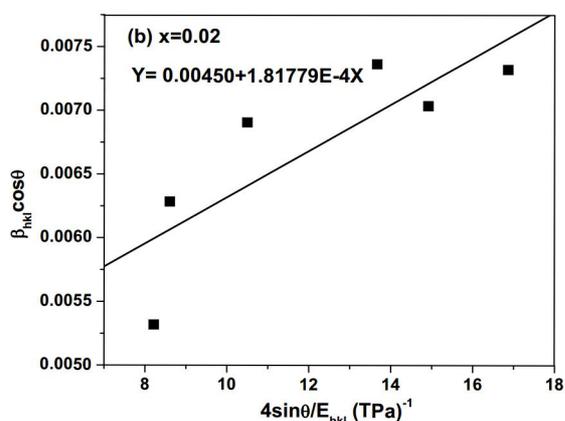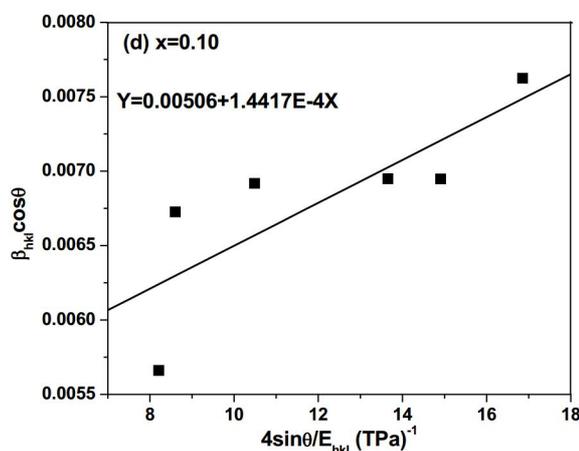Fig. 4(c).

Fig. 4(b).

Fig. 4(d)

Fig. 4(a-d). The plots $\beta_{hkl}\cos\theta$ Vs $4\sin\theta/E_{hkl}$ of $Zn_{1-x}Mn_xO$ samples.

deformation can be determined from the slope of the line drawn between $\beta_{hkl}\cos\theta$ and $4\sin\theta$ $(2/E_{hkl})^{1/2}$. The lattice strain of the sample is calculated from known values of young's modulus. It is confirmed that the values of energy density and stress are related with UDSM and UDEDM. The anisotropic nature of the crystallite is given by the equations (6) and (8). It is well understood that the equations (6) and (8) give the $u = \sigma^2/E_{hkl}$ between deformation stress and energy density of crystallites. The stress and energy density first increases up to x= 0.02 and then decrease with increasing Mn concentration are shown in figure 7.

It is noticed that the elastic constant has different anisotropic behavior. It is considered from the equation (3) that the deformation stress has the same value along all crystallographic directions which exhibits u is the anisotropic. Whereas equation (8) gives deformation energy along all crystallographic directions is uniform considering the deformation stress σ is uniform. Hence it is well noticed that for lattice strain and crystallite size, the Williamson-Hall modified equations (6) and (8) & their plots give the different values. W-H plots of annealed $Zn_{1-x}Mn_xO$ nanocrystals are plotted using equations (1–8) and selected most suitable
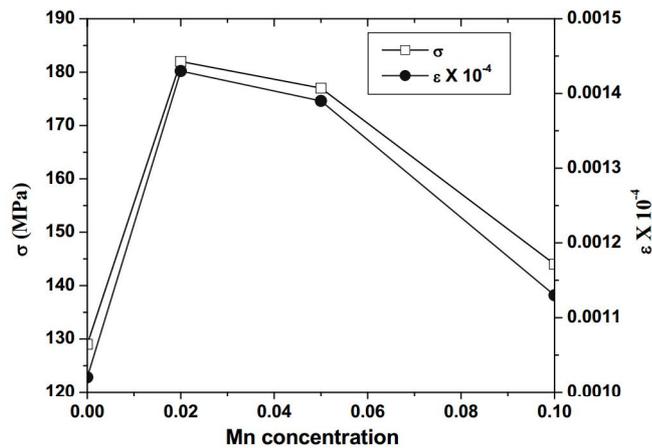
82

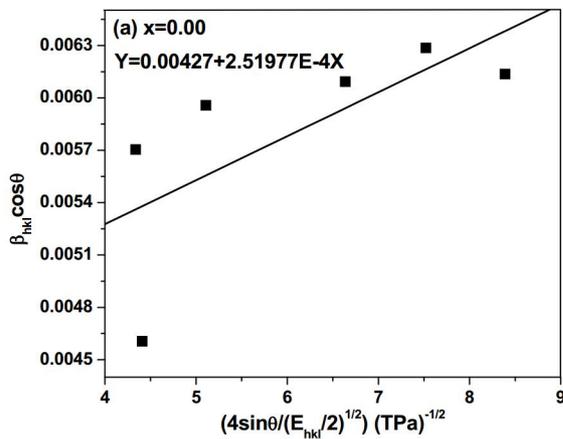**Fig. 5.** Stress and strain versus Mn concentration of $Zn_{1-x}Mn_xO$ samples.
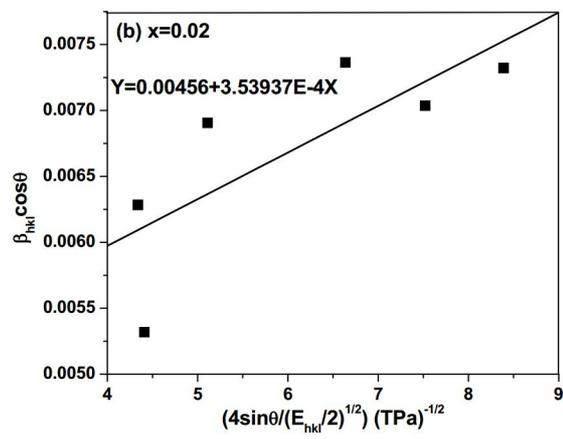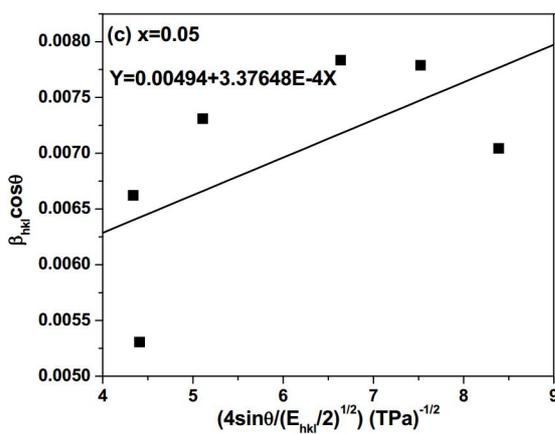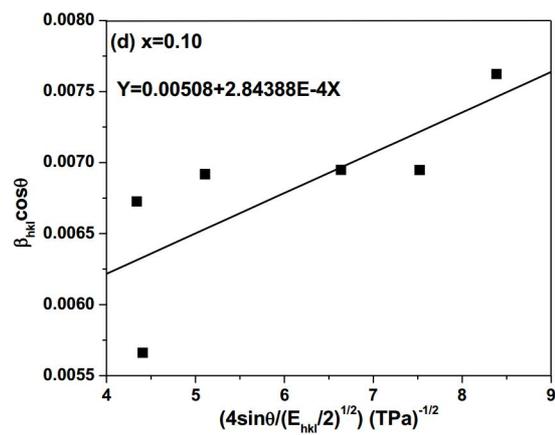

Fig. 6(a).

Fig. 6(b).

Fig. 6(c).

Figure 6(a-d). The plots $\beta_{hkl}\cos\theta$ Vs $4\sin\theta(2/E_{hkl})^{1/2}$ of $Zn_{1-x}M$

Fig. 6(a-d). The plots $\beta_{hkl}\cos\theta$ Vs $4\sin\theta(2/E_{hkl})^{1/2}$ of $Zn_{1-x}Mn_xO$ samples.

83

models which give a linear fit of the experimental data. Figure 4 (a-d) shows the comparison of the three models for $Zn_{1-x}Mn_xO$ nanocrystals. It is observed from figures 2(a-d), 4(a-d) and 6(a-d) points are less scattered for figures 2(a-d) as compared to figures 4(a-d) and 6(a-d). The average crystallite size was estimated using figures 2(a-d), 4(a-d) and 6(a-d) from the Y-intercept of the plots are in the range of 26 - 33 nm. The values evaluated using these three models are in good agreement with the TEM results. One may say that in the present study these models are realistic. Yogamalar et. al. [15] and Zak et. al. [16] have reported for pure ZnO samples at different temperature, it is noticed that their values of crystallite size calculated by Scherrer's formula and by three models are not matchable. They did not work for Mn concentration and not studied the effect of Mn doping whereas we have studied the effect of Mn substituted on ZnO nanocrystals. When Mn concentration increases the crystallite size decreases, it may be owing to the higher ionic radii of Mn than Zn and sintering temperature. This study throws light and reveals the importance of models in the determination of crystallite size of pure and Mn substituted ZnO nanocrystals. We suggest that these three models are the best models for the evaluation of crystallite size of pure and Mn substituted ZnO

nanocrystals. In our case all three models are found suitable for the determination of crystallite size.

Using eq. (7), The Young's modulus of the annealed ZnO sample was evaluated to be ~127GPa and it is in a good matching with the reported literature [16]. Geometric parameters of annealed pure and Mn substituted ZnO samples obtained from TEM, XRD and UDM, UDSM, UDEDM are listed in table 2. The average crystallite size was estimated using these UDM, UDSM and UDEDM are comparatively equal which indicate the inclusion of strain. Using Scherrer's formula and W-H analysis, average crystallite size was estimated and noticed that small variation is due to the difference in averaging the particle distribution. Using different forms of the W-H analysis, the average crystallite size and strain values estimated by plotting the graphs were confirmed to be almost similar and comparable. We have calculated the crystallite size of pure ZnO sample by Scherrer's formula and using three models, it is highly matchable. Same trend found for Mn doping too, it may be due to suitable sintering temperature and ionic radii of Mn.

3. 3. TEM Measurements of $Zn_{1-x}Mn_xO$ Nanocrystals
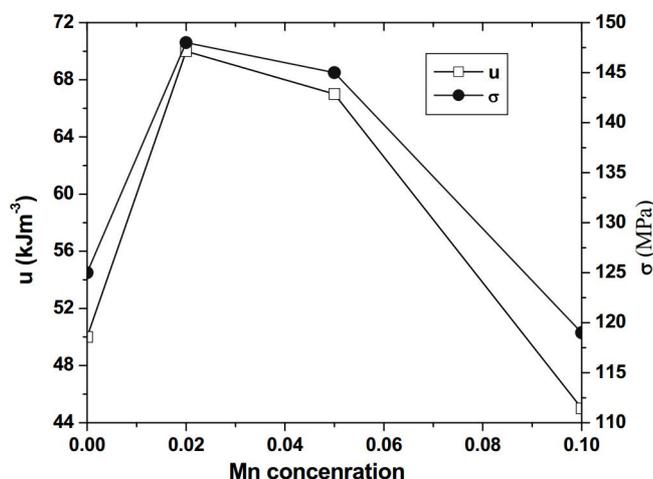
Figure 8 exhibits the TEM image of the ZnO

Fig. 7. Energy density and stress versus Mn concentration of $Zn_{1-x}Mn_xO$ samples.
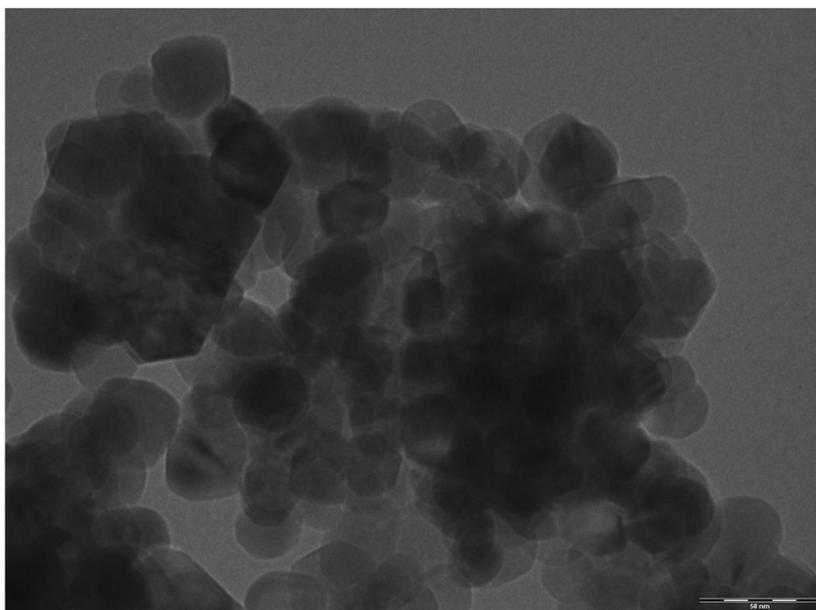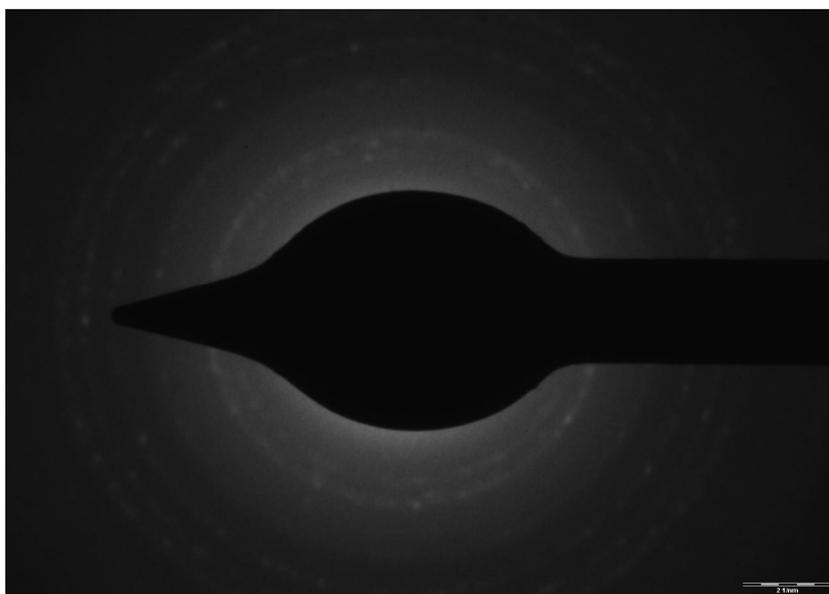
Fig. 8. TEM image of ZnO sample.

Fig. 9. Selected area electron diffraction (SAED) patterns of ZnO sample.

sample at room temperature. It is noticed that the TEM image shows clearly nanocrystalline nature of the sample. Figure 9 shows the SAED image of the ZnO sample.

In case of TEM technique, the electromagnetic lines of electron beams are passed through a sample of annealed ZnO sample at 450 °C. The mean size of the particle is measured from direct TEM technique is approximately 20-60 nm. The TEM image shows that the ZnO sample has crystalline nature with wurtzite structure and no extra impurity phases were detected. Typical
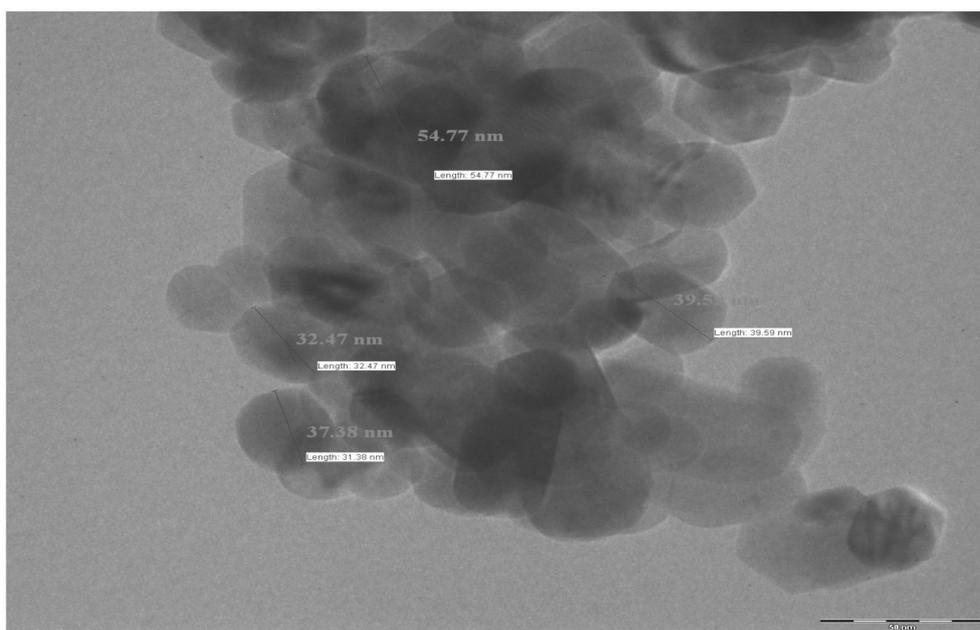
85

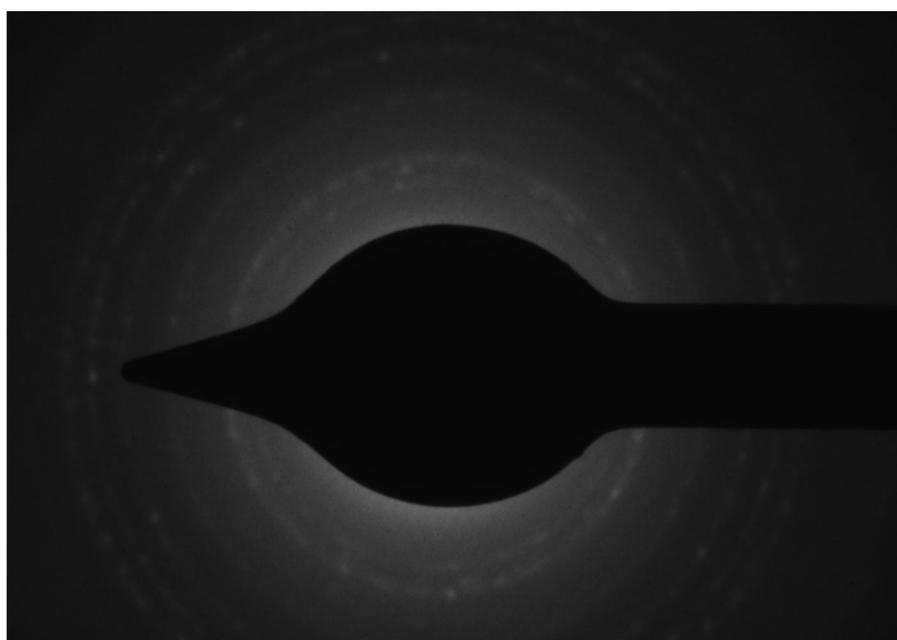**Fig. 10.** TEM image of Mn substituted ZnO sample.

Fig. 11. Selected area electron diffraction (SAED) patterns of Mn substituted ZnO sample.

TEM micrograph of Mn substituted ZnO (x = 0.10) nanoparticles is shown in figure 10. These nanoparticles are nearly spherical in shape and have an average particle size about 20 - 50 nm, which is in good agreement with the value obtained from XRD analysis but in reported literature [17] difference is found. Most of the crystalline of pure ZnO is nearly in hexagonal shape and Mn doped ZnO are in spherical shape. The existence of Mn caused the cross-sections of

86

few nanoparticles to change from hexagonal to spherical shape. It means Mn goes to the Zn sites of ZnO wurtzite structure.

The figure 11 presents a spotted ring like SAED (selected area electron diffraction) pattern decorated with random bright spots which demonstrate that the particles have a polycrystalline like structures. The selected area electron diffraction (SAED) pattern consists of nine concentric sharp rings, which corresponded to the (100), (002), (101), (102), (110), (103), (200), (112) and (201) of the diffraction of the ZnO in the wurtzite structure. Therefore, it can be further confirmed that the nanoparticles are in the hexagonal (wurtzite) structure. Other secondary phases are not observed in the figure. It means the Mn ions are diluted in the ZnO matrix. No notable contrast is induced by the interstitial Mn in the ZnO matrix. It indicates that Mn atoms may be mainly located at substitution sites. These results are in good agreement with the XRD results and confirm absence of secondary phases upto $x = 0.10$.

4. CONCLUSION

Nanocrystals of pure and manganese substituted ZnO were prepared by the co-precipitation technique. The X-ray diffraction analysis of these samples shows wurtzite (hexagonal) structure of ZnO. The volume of unit cell increases with increasing Mn content is observed for Mn doped ZnO samples. It indicates that Mn ions go to the Zn sites in the ZnO lattice structure. The X-ray density decreases with increasing Mn content, it may be due to the reduction in the molecular weight of the samples. The average crystallite size was obtained from the width of X-ray diffraction lines using Scherrer's formula; it is found that average crystallite size decreases with increasing Mn content. The particle size and morphology of the $Zn_{1-x}Mn_xO$ nanocrystals have been determined by transmission electron microscopy. It exhibits that the particle lies in the size range 20 - 60 nm which is consistent with the result obtained for particle size from the width of XRD peaks broadening. The selected-area electron diffraction (SAED) pattern shows that the nanoparticles are crystalline in nature. The crystallite size and lattice strain contributions to peak broadening were analyzed using three different models of W–H analysis. The value of crystallite size calculated from the three models of the W–H analysis is in agreement with that of the average crystallite size measured from TEM. We suggest that this model may be employed in nanomaterials and nanotechnology for determination of crystallite size and strain which gives new direction for researchers and technologists.

REFERENCES

1. Harbour, J. R., Hair, M. L., "Radical intermediates in the photosynthetic generation of hydrogen peroxide with aqueous zinc oxide dispersions", J. Phys. Chem.,1979, 83, 652.
2. Mitra, P., Chatterjee, A., Maiti, H., "ZnO thin film sensor", Mater. Lett., 1998, 35, 33.
3. Gupta, T. K., "Application of Zinc Oxide Varistors", J. Am. Ceram. Soc., 1990, 73, 1817.
4. Dijken, A. V., Mulenkamp, E. A., Vanmaekelbergh, D., Meijerink, A., "Identification of the transition responsible for the visible emission in ZnO using quantum size effects", J. Lumin., 2000, 90, 123.
5. Sakohara, S., Tickazen, L. D., Anderson, M. A., "Luminescence properties of thin zinc oxide membranes prepared by the sol-gel technique: change in visible luminescence during firing", J. Phys. Chem., 1992, 96, 11086.
6. Ramakanth, K., "Basics of X-ray Diffraction and its Application", I. K. International Publishing House Pvt. Ltd., New Delhi, 2007, pp. 272.
7. Ungar, T., "Characterization of nanocrystalline materials by X-ray line profile analysis", J. Mater. Sci., 2007, 42, 1584.
8. Suryanarayana, C., "Mechanical Alloying and Milling", Marcel Dekker, New York, 2004, pp. 466.
9. Suryanarayana, C., Grant Norton, M., "X-ray Diffraction: A Practical Approach", New York, 1998, pp. 207-222.
10. Zhang, J., Zhang, Y., Xu, K. W., Ji, V., "General compliance transformation relation and applications for anisotropic hexagonal metals", Solid State Commun., 2006, 139, 87.

11. Balzar, D., Ledbetter, H., "Voigt-function modeling in Fourier analysis of size- and strain-broadened X-ray diffraction peaks", J. Appl. Crystallogr., 1993, 26, 97.

12. Warren, B. E., Averbach, B. L., "The Effect of Cold Work Distortion on X-Ray Patterns", J. Appl. Phys., 1950, 21, 595.

13. Nye, J. F., "Physical Properties of Crystals: Their Representation by Tensors and Matrices", Oxford, New York, 1985, pp. 329.

14. Yousefi, R., Zak, A. K., Jamil-Sheini, F., "Growth, X-ray peak broadeninig studies, and optical properties of Mg-doped ZnO nanoparticles", Materials Science in semiconductor processing, 2013, 16, 771.

15. Yogamalar, R., Srinivasan, R., Vinu, A., Ariga, K., Bose, A. C., "X-ray peak broadening analysis in ZnO nanoparticles", Solid State Communications, 2009, 149, 1.

16. Zak, A. K, Majid, W. H., Abd, Abrishami, M. E., Yousefi, R., "X-ray analysis of ZnO nanoparticles by Williamson-Hall and sizs-strain plot methods", Solid State Commun, 2011, 13, 251.

17. Yousefi, R., Zak, A. K., Jamali-Sheini, F., "The effect of group-I elements on the structure and optical properties of ZnO nanoparticles", Ceramics International, 2013, 39, 1371.